Chemical Geology 368 (2014) 63–75

Contents lists available at ScienceDirect

Chemical Geology

journal homepage: www.elsevier.com/locate/chemgeo

Simultaneous precipitation of magnesite and lizardite from hydrothermal alteration of olivine under high-carbonate alkalinity

Romain Lafay [a,b], German Montes-Hernandez [a,*], Emilie Janots [b], Rodica Chiriac [c], Nathaniel Findling [b], François Toche [c]

[a] CNRS, ISTerre, F-38041 Grenoble, France
[b] Univ. Grenoble Alpes, ISTerre, F-38041 Grenoble, France
[c] Université de Lyon, Université Lyon 1, Laboratoire des Multimatériaux et Interfaces UMR CNRS 5615, 43 bd du 11 novembre 1918, 69622 Villeurbanne Cedex, France

ARTICLE INFO

Article history:
Received 17 June 2013
Received in revised form 10 January 2014
Accepted 13 January 2014
Available online 21 January 2014

Editor: J. Fein

Keywords:
Olivine alteration
High-carbonate alkalinity
Magnesite
Lizardite
Crystal growth
Hydrothermal systems

ABSTRACT

The present study reports original experiments in order to investigate the simultaneous serpentinization and carbonation of olivine with relevance in Earth systems (e.g. functioning of hydrothermal fields) or in engineered systems (e.g. ex-situ and in-situ mineral sequestration of CO_2). For this case, specific experimental conditions were examined (200 °C, saturated vapor pressure ≈ 16 bar, solution/solid weight ratio = 15, olivine grain size < 30 μm and high-carbonate alkalinity ≈ 1 M $NaHCO_3$). Under these conditions, competitive precipitation of magnesite and serpentine (preferentially lizardite type) was clearly determined by using conventional analytic tools (XRD, FESEM, FTIR and TGA); excluding the fate of the iron initially contained in olivine, the alteration reaction for olivine under high-carbonate alkalinity can be expressed as follows:

$$2Mg_2SiO_4 + 2H_2O + HCO_3^- \rightarrow MgCO_3 + Mg_3Si_2O_5(OH)_4 + OH^-.$$

This reaction mechanism implied a dissolution process, releasing Mg and Si ions into solution until supersaturation of solution with respect to magnesite and/or serpentine. The released iron contained in the olivine has not implied any precipitation of iron oxides or (oxy)hydroxides; in fact, the released iron was partially oxidized (about 50%) via a simple reduction of water ($2Fe^{2+} + 2H_2O \rightarrow 2Fe^{3+} + H_2 + 2OH^-$). In this way, the released iron was incorporated in serpentine (Fe(II) and Fe(III)) and in magnesite (Fe(II). The latter was clearly determined by FESEM/EDS chemical analysis on the single magnesite crystals. The nucleation and epitaxial growth processes at the olivine–fluid interfaces cannot be excluded in our investigated system.
The experimental kinetic data fitted by using a kinetic pseudo-second-order model have revealed a retarding process of serpentine formation with respect to magnesite (about three times slower); in fact, the magnesite seems to reach an apparent stabilization after about 20 days of reaction while the serpentine follows a progressive slower evolution. We assumed that the magnesite has reached a fast apparent equilibrium with solution because the available carbonate species are not renewed from fluid phase as typically constrained in aqueous carbonation experiments where a given CO_2 pressure is imposed in the system.
On the other hand, the reactivity of serpentinized olivine (chrysotile + brucite + small amount of residual olivine) and high-purity chrysotile at the same above investigated conditions; and the olivine serpentinization in initial acid pH ≈ 0.66 are also reported as complementary information in this study.
These novel experimental results concerning simultaneous serpentinization and aqueous carbonation of olivine expand the thermodynamic conditions where serpentine and magnesite can simultaneously precipitate; this could contribute to a better understanding of fluid–rock interactions in natural active hydrothermal fields on Earth.

1. Introduction

The physicochemical reactions at the solid–fluid interfaces play a crucial role in the global cycle of major and trace elements in the Earth and other telluric planets. In this way, chemical weathering, metamorphic reactions, diagenetic reactions, hydrothermalism, volcanic activity, and crystal–melt reactions are important non-limited physicochemical processes that shape the Earth's surface and sub-surface. However, many physicochemical and textural aspects of these so-called rock–fluid interactions are still poorly understood. For example, when mantle peridotite is tectonically exposed with (sub-)surface fluids (e.g. seafloor water and meteoric water), the olivine and pyroxene anhydrous minerals contained in peridotite are far-from-equilibrium with respect to fluid composition. In this way, numerous physicochemical reactions at peridotite–fluid interfaces can take place such as hydration (–OH

* Corresponding author.
E-mail address: german.montes-hernandez@ujf-grenoble.fr (G. Montes-Hernandez).

0009-2541/$ – see front matter © 2014 Elsevier B.V. All rights reserved.
http://dx.doi.org/10.1016/j.chemgeo.2014.01.008

incorporation or serpentinization) and carbonation processes if the required temperature and fluid compositions are enough to activate these reactions; both most important processes directly related to natural H_2 and abiotic methane production via redox reactions and the formation of other non-limited secondary minerals as it has been observed in various natural hydrothermal sites (e.g. Logatchev, Rainbow and The Lost City) (e.g. Charlou et al., 2002; Allen and Seyfried, 2004; Ludwig et al., 2006; Seyfried et al., 2007; Klein et al., 2009; McCollom and Bach, 2009; Rudge et al., 2010; Seyfried et al., 2011). Such reducing systems may represent analogs to early Earth environments and may provide insights into requirements for the emergence of life, probably initiated at the sea floor (e.g. MacLeod et al., 1994; Charlou et al., 2002; Früh-Green et al., 2003; Kelley et al., 2005). The field monitoring and ex-situ characterization have revealed complex fluid chemistry and generally low pH (from 2.8 to 4.3) and high temperature (from 275 to 365 °C) in the expelled fluids from various studied ultramafic-hosted hydrothermal systems at the Mid-Atlantic Ridge (Charlou et al., 2002). Conversely, the expelled fluids at the Lost City field and other sites for example in continental serpentinization systems (e.g. Samail Ophiolite in Oman) are highly alkaline (pH > 9) and lower temperatures have been monitored/determined (from 55 to 90 °C) (Kelley et al., 2001; Früh-Green et al., 2003; Ludwig et al., 2006; Kelemen et al., 2011). These surprising measurements and the recent discovery of spectacular carbonate towers at the Lost City hydrothermal field have stimulated interest in the role of serpentinization and carbonation processes on the production of hydrogen- and methane-rich fluids and on the biological communities that may be supported in these environments (Früh-Green et al., 2003; Kelley et al., 2005; Schrenk et al., 2013). Moreover, at the present time, the ex-situ and in-situ carbonation of mafic and ultramafic rocks (e.g. basalts and peridotite), extensively available in the oceanic crust and ophiolites, have been proposed as a promising solution to mitigate the global warming of Earth's atmosphere related to excessive anthropogenic and natural CO_2 emissions; because Mg-, Ca- or Fe-carbonates resulting from mineral carbonation of CO_2 can remain stable at the geological time scales as frequently observed in the Earth surface and/or sub-surface (e.g. Seifritz, 1990; Lackner et al., 1995; Bachu, 2000; Kaszuba et al., 2003; Xu et al., 2004; Kaszuba et al., 2005; Gerdemann et al., 2007; IPCC, 2007; Kelemen and Matter, 2008; Oelkers et al., 2008; Matter and Kelemen, 2009; Montes-Hernandez et al., 2009a, 2009b; Kelemen et al., 2011; Schwarzenbach et al., 2013). In this general context, numerous experimental studies concerning the serpentinization or carbonation of peridotite (or single olivine) have been recently performed using batch, semi-continuous or flow-through reactors in order to better understand the reaction mechanisms and kinetics, reaction and cracking propagation from the grain boundaries, nature and role of secondary phase formation, potential of hydrogen production, potential for mineral sequestration of CO_2 and role of P, T, pH, solid/fluid ratio and fluid chemistry (e.g. Wunder and Schreyer, 1997; James et al., 2003; Giammar et al., 2005; Bearat et al., 2006; Seyfried et al., 2007; Andreani et al., 2009; McCollom and Bach, 2009; Garcia et al., 2010; King et al., 2010; Daval et al., 2011; Hövelmann et al., 2011; Klein and Garrido, 2011; Marcaillou et al., 2011; Bonfils et al., 2012; Lafay et al., 2012; Malvoisin et al., 2012). However, the competitive and/or coexistence between serpentinization and carbonation at peridotite–fluid interfaces have been rarely investigated at the laboratory scale, remarking that serpentinization and carbonation of peridotite, leading to precipitation of serpentine (e.g. lizardite and chrysotile) and magnesite (or hydrated Mg carbonates), could occur simultaneously in natural hydrothermal systems if the interacting solution is supersaturated with respect to both minerals. For this simple reason, the main goal of this present study was focussed to determine the simultaneous precipitation of serpentine and magnesite from hydrothermal alteration of olivine under high-carbonate alkalinity. For this particular case, specific experimental conditions were used (200 °C, saturation vapor pressure (≈16 bar), solution/solid weight ratio (=15), olivine grain size (<30 μm) and high-carbonate alkalinity solution (1 M $NaHCO_3$)). These experimental conditions were selected with help of previous-experimental studies, investigating independently the serpentinization or the carbonation of olivine (e.g. Giammar et al., 2005; Bearat et al., 2006; Seyfried et al., 2007; Garcia et al., 2010; King et al., 2010; Daval et al., 2011; Hövelmann et al., 2011; Marcaillou et al., 2011; Bonfils et al., 2012; Lafay et al., 2012; Malvoisin et al., 2012). High-purity synthetic chrysotile and serpentinized olivine (chrysotile + brucite mineral + small amount of residual olivine) obtained in our laboratory were also used as starting solids in complementary-similar experiments in order to determine their reactivity under high-alkalinity. As expected, the chrysotile was slightly altered and brucite quickly transformed to magnesite at the investigated conditions. Various analytical tools such as X-ray diffraction (XRD), Field Emission Gun Scanning Electron Microscopy (FESEM), Thermogravimetric analyses (TGA/SDTA) and Fourier Transform Infrared Spectroscopy (FTIR) were used to characterize the solid products. TGA analyses and the respective 1st derivative curves were particularly used to determine with high accuracy the temporal variation of magnesite and serpentine during olivine alteration.

2. Materials and methods

2.1. Preparation of solid reactants

2.1.1. Olivine grains

Millimetric grains of olivine San Carlos (Fo_{91}) were crushed using a Fritsh Pulverisette 7 micro-crusher. One class of grain/particle size (particle size < 30 μm) was isolated by sieving. The samples were washed three times using high-pure water in order to remove the ultrafine particles that possibly stuck at grain surfaces during crushing step. Optical and electron microscopy was performed to control the initial state/appearance of olivine surfaces. On the other hand, high specific surface area (2.3 $m^2\ g^{-1}$) was deduced from N_2 adsorption isotherm using conventional Brunauer–Emmett–Teller (BET) method. This high specific surface area was probably due to a significant presence of very fine particles (<1 μm; not verified), not spherical morphology of grains and significant surface-defaults and/or roughness.

2.1.2. High-purity synthetic chrysotile

250 ml of 1 M NaOH solution, 1.302 g of silica gel (H_2SiO_3) and 5.082 g of magnesium chloride hexahydrate ($MgCl_2 \cdot 6H_2O$) were placed in a Parr *copper alloy* reactor (autoclave with internal volume of 0.5 L). This aqueous reactive system was immediately stirred using constant mechanical agitation (300 rpm) during the reaction. The aqueous system was then heated at 300 °C for 30 h by using a heating jacket adapted to the reactor. Based on several previous experiments, these experimental conditions were optimal to synthesize high-purity chrysotile with high specific surface area (S_{BET} = 185 $m^2\ g^{-1}$), more specifically a mesoporous material (pore size 2 to 50 nm) (Lafay et al., 2013).

2.1.3. Serpentinized olivine (chrysotile + brucite + small amount of residual olivine)

Micrometric grains of olivine (<30 μm) were altered in concentrated NaOH solution (1 M) at 200 °C in static batch mini-reactors for 30 days. 30 days of olivine–fluid interactions were enough to obtain almost complete mineral replacement of olivine to chrysotile and brucite. This implied a spatial and temporal coupling of dissolution and precipitation reactions at the interface between olivine and chrysotile–brucite minerals. This coupled dissolution–precipitation led to the alteration of starting olivine grains (so-called primary or parent mineral) to a porous mineral assemblage of chrysotile and brucite with preservation of the initial olivine grain shape. For more specific details on the olivine replacement by chrysotile and brucite, including kinetics and reaction steps, refer to Lafay et al. (2012).

2.2. Preparation of reacting solutions

2.2.1. High-alkaline $NaHCO_3$ solution (S1)

This alkaline solution was recovered from magnesite synthesis that has used $Mg(OH)_2$ (1 mol), NaOH (2 mol), high-purity H_2O (1 L) and CO_2 (50 bar equivalent to 2 mol in the reactor) as reactants. More details on this synthesis method and recovery of alkaline solution by centrifugation can be found in Montes-Hernandez et al. (2012a,b). In summary the recovered solution has a pH of 8.9 (measured at ~20 °C), a high concentration of total carbon (=1 M) measured by TOC-V_{CSN} analyzer and low concentration of Mg (~250 mg l^{-1}) measured by ICP-OES. Assuming that all dissolved carbon comes from injected CO_2, the Phreeqc equilibrium modeling (Parkhurst and Appelo, 1999) confirms that the recovered solution is enriched particularly with $NaHCO_3$ (~1 M).

2.2.2. High-alkaline $NaHCO_3$ solution (S2)

This solution was obtained by direct capture of CO_2 via ionic dissociation in a concentrated NaOH solution (2 M). Herein, 50 bar of CO_2 (~2 mol) were injected into the reaction titanium cell (2 L of volume) at ambient temperature (~20 °C). The CO_2 consumption (or pressure drop of CO_2) and temperature (exothermic reaction) were in-situ monitored until a macroscopic equilibrium that was reached after about 24 h. Then, the residual CO_2 gas was removed from reactor and the solution was recovered by simple decanting of supernatant solution. Based on Solvay typical reactions, the following global reactions are expected:

$$2NaOH + CO_2 \rightarrow Na_2CO_3 + H_2O \quad (1a)$$

$$Na_2CO_3 + H_2O + CO_2 \rightarrow 2NaHCO_3. \quad (1b)$$

The X-ray diffraction on the recovered solid and the measurements in the solution (pH = 8.7 and TC = 0.95 M) have confirmed this above reactions.

2.3. Serpentinization–carbonation experiments

In each experiment 1.5 ml of high-alkaline solution (S1 or S2) and 100 mg of olivine (grain size < 30 μm) were placed in a Teflon cell reaction (cap-cell also in Teflon). Cell reaction and cap-cell were previously washed by an acidic treatment followed by washing with high-pure water. This cell reaction was immediately assembled into a steel autoclave without agitation, referred to as "static batch reactor" and the closed autoclave was placed in a multi-oven (ten independent-temperature compartments) and heated to 200 °C ($P_{sat} \approx 16$ bar). Various olivine–fluid reaction times from 3 h to 60 days were considered in order to determine the serpentinization and carbonation rates of olivine at the investigated hydrothermal conditions. Complementary experiments were carried out at the same experimental conditions. Herein, serpentinized olivine (chrysotile + brucite + small amount of residual olivine) was reacted with S1 solution (runs: 11 to 15) and high-purity synthetic chrysotile was also reacted with S1 solution (runs: 6 to 10). All experiments or runs and some results are summarized in Table 1.

At the end of the experiment, the autoclave was quenched in cold water and then disassembled. The quenching step avoids a significant perturbation of solid reaction products. Conversely, the chemistry of recovered solutions (pH, ion composition and probably ion speciation) can be significantly modified by cooling and/or depressuring processes as clearly demonstrated by modeling for calcite precipitation under hydrothermal conditions (Fritz et al., 2013). For this reason, the olivine alteration was directly deduced from solid mineral characterization in this present study. Moreover, for batch experiments, the ion composition and/or concentration are not directly related to alteration extent for a given mineral(s). In summary, only the pH into the collected solutions was measured at room temperature (≈20 °C) "not representative of in-situ pH during olivine alteration", these results are also summarized in Table 1. The solid product was systematically washed in 25 ml of high-purity water and separated by centrifugation. Finally, the solid product was directly dried in the centrifugation flask at 90 °C for 24 h. The dry solid product was recovered for further solid characterizations described below.

Table 1
Summary of experimental conditions and thermogravimetric analyses (TGA).

Run #	Starting material	Time (days)	Solution	pH		Product amount (%) from TGA			
				Initial	Final	Serpentine	Magnesite	Brucite	Residual olivine
1	Ol	3	S1	8.9	9.17	4.0	12.8	–	83.2
2	Ol	10	S1	8.9	9.38	21.6	14.9	–	63.5
3	Ol	20	S1	8.9	9.63	18.5	25.5	–	56.0
4	Ol	33	S1	8.9	9.55	27.0	23.7	–	49.3
5	Ol	60	S1	8.9	9.58	40.6	26.6	–	32.8
6	Ctl	3	S1	8.9	9.05	95.4	4.6	–	–
7	Ctl	11	S1	8.9	9.18	95.4	4.6	–	–
8	Ctl	22	S1	8.9	9.25	95.8	4.2	–	–
9	Ctl	32	S1	8.9	9.19	95.7	4.3	–	–
10	Ctl	78	S1	8.9	8.83	96.8	3.2	–	–
11	Ctl + bru	3	S1	8.9	9.57	82.9	17.1	–	–
12	Ctl + bru	10	S1	8.9	9.57	82.6	17.4	–	–
13	Ctl + bru	20	S1	8.9	9.59	83.6	16.4	–	–
14	Ctl + bru	33	S1	8.9	9.58	81.3	18.7	–	–
15	Ctl + bru	60	S1	8.9	9.66	79.0	21.0	–	–
16	Ol	3	S2	8.7	9	2.8	10.1	–	87.0
17	Ol	10	S2	8.7	9.4	19.6	16.6	–	63.8
18	Ol	20	S2	8.7	9.45	26.7	22.8		50.5
19	Ol	23	S2	8.7	9.49	24.8	20.9	–	54.4
20	Ol	60	S2	8.7	9.57	46.7	23.0	–	30.3
21	Ol	10	S3	0.63	4.77	3.8	–	< 1	96.2
22	Ol	66	S3	0.63	6.37	14.5	–	< 1	85.5
23	Ol	90	S3	0.63	7.29	33.1	–	5	62.9
24	Ol	183	S3	0.63	7.95	71.4	–	7.9	20.7

All experiments were carried out at 200 °C and saturated vapor pressure. Fluid/solid weight ratio is always ≈15. S1 and S2 are high-carbonate alkalinity solutions (≈1 M $NaHCO_3$). S3 is an acid solution (pH ≈ 0.63) prepared by dilution of concentrated HCl solution (10% v/v). pH is ex-situ measured at room temperature ≈ 20 °C. Ol: olivinie; Ctl: chrysotile; bru: brucite.

2.4. Serpentinization in initial acid pH

Similar to above alteration procedure was performed to investigate the effect of initial acid pH on the serpentinization process. For this case, the olivine grains (<30 μm) were exposed in HCl solution (S3) (initial pH = 0.63) at different duration times (10, 66, 90 and 180 days). These batch experiments are also summarized in Table 1.

2.5. Characterization of solid products

The following four conventional techniques were used in complementary manner to determine the mineral composition, morphology of crystals and serpentine polymorphs of reacted samples.

2.5.1. FESEM observations

Serpentinized-carbonated materials were dispersed by ultrasonic treatment in absolute ethanol (chemical purity > 98%) for 5 to 10 min. One or two droplets of the suspension were then deposited directly on an aluminum support for SEM observations, and coated with platinum. The morphology of various selected powders was observed using a Zeiss Ultra 55 field emission gun scanning electron microscope (FESEM) with a maximum spatial resolution of approximately 1 nm at 15 kV.

2.5.2. XRD measurements

X-ray Powder Diffraction (XRD) analyses were performed using a Siemens D5000 diffractometer in Bragg–Brentano geometry; equipped with a theta–theta goniometer with a rotating sample holder. The XRD patterns were collected using Cu $k\alpha_1$ ($\lambda_{k\alpha1}$ = 1.5406 Å) and $k\alpha_2$ ($\lambda_{k\alpha2}$ = 1.5444 Å) radiation in the range 2θ = 10–70° with a step size of 0.04° and a counting time of 6 s per step.

2.5.3. Thermogravimetric analyses

TGA for all serpentinized-carbonated samples were performed with a Mettler Toledo TGA/SDTA 851e instrument under the following conditions: sample mass of about 10 mg, 150 μl alumina crucible with a pinhole, heating rate of 10 °C min^{-1}, and inert N_2 atmosphere of 50 ml min^{-1}. Sample mass loss and associated thermal effects were obtained by TGA/SDTA. In order to identify the different mass loss steps, the TGA first derivative (rate of mass loss) was used. The TGA apparatus was calibrated in terms of temperature. The melting points of three compounds (indium, aluminum and copper) obtained from the DTA signals were used for the sample temperature calibration.

2.5.4. FTIR measurements

Infrared measurements (in transmission mode) were performed using an IR microscope Bruker Hyperion 3000. The IR beam was focused through a 15× lens and the typical size of infrared spot is 50 × 50 mm^2. The light source is a Globar (TM) and the beam splitter is in KBr. The spectra were measured from 700 to 4000 cm^{-1} (4 cm^{-1} resolution) with a MCT monodetector cooled by liquid nitrogen. Samples must be thin (less than 100 μm) and flat to avoid absorption band saturation or scattering effects. Sample preparation has involved a careful crushing of samples in mortar and manual compaction of fine crushed particles between two KBr windows. In general, five spectra per sample were collected in different zones and/or aggregates in order to verify their homogeneity/discrepancy.

3. Results

3.1. Mineral composition of products

The conventional analytic techniques (XRD, TGA, FTIR and FESEM) have revealed that the hydrothermal alteration of olivine using high-carbonate alkalinity solutions, i.e. enriched with CO_2 (S1 and S2 solutions), concerns the competitive formation of magnesite and serpentine, in other words, competitive carbonation and serpentinization processes during olivine alteration was clearly observed. As expected, both solutions (S1 and S2) have revealed a very similar effect on the olivine alteration because the mineral composition of products and alteration extent were not significantly affected for comparable samples. For specific details, refer to mineral composition evolution summarized in Table 2 for runs 1 to 5 and 16 to 20. Herein, magnesite was observed from 3 days of reaction until the end of experiment (60 days). Conversely, the formation of serpentine (preferentially lizardite type) was retarded with respect to magnesite because it was clearly identified by X-ray diffraction after 10 days of reaction. Chrysotile tubes were also observed by FESEM, preferentially after 30 days reaction. All these qualitative results are summarized in Fig. 1, displaying some XRD patterns and some FESEM images for collected products as the function of reaction time. We note that the experimental duration of 60 days were not enough to transform the available olivine completely into magnesite and serpentine as qualitatively determined by X-ray diffraction (see XRD pattern after 60 days in Fig. 1) and by infrared spectroscopy (Fig. 2). This latter analytical tool has confirmed a preferential formation of lizardite polymorph as attested by their two typical stretching infrared modes at 966 and 1085 cm^{-1} for Si–O group (see Fig. 2b). These infrared features are clearly different to infrared features of chrysotile polymorph (Fig. 2c). We also remark that infrared features are in agreement with FESEM observations, which reveal fine particles with platy morphology for lizardite (Fig. 1c) and typical tubular morphology for chrysotile (Fig. 1d). In an effort to quantify "with high-accuracy" the co-formed amount of magnesite and serpentine as a function of time, the thermogravimetric analysis (TGA) were performed at a specific heating rate of 10 °C min^{-1} under 100% N_2 atmosphere (see materials and methods section for more specific details). Herein, the first derivative curve (DTG) was successfully used to delimit the magnesite and serpentine contents for each reaction-time sample as illustrated in Fig. 3. All calculated relative-values for magnesite and serpentine are summarized in Table 1 and they were also used to determine the

Table 2
Summary of kinetic parameters for simultaneous serpentinization and aqueous carbonation of olivine, including alteration of olivine under high carbonate and hydroxyl alkalinity.

Process	$\xi_{extent,max}$ (%)	$t_{1/2}$ days	v_0 1/s	R^2
$2Mg_2SiO_4 + 2H_2O + HCO_3^- \rightarrow MgCO_3 + Mg_3Si_2O_5(OH)_4 + OH^-$				
Serpentine formation	65 ± 13	33 ± 13.4	2.3×10^{-7}	0.90
Magnesite formation	27 ± 1.7	4.8 ± 1.3	6.5×10^{-7}	0.85
Alteration	81 ± 5.2	14 ± 2.5	$6.6 \times 10^{-7} = 1.8636 \times 10^{-9}$ mol m^{-2} s^{-1}	0.96
$2Mg_2SiO_4 + 3H_2O \rightarrow Mg(OH)_2 + Mg_3Si_2O_5(OH)_4$				
Alteration	105 ± 5.5	2 ± 0.46	$5.9 \times 10^{-6} = 1.6659 \times 10^{-8}$ mol m^{-2} s^{-1}	0.96
Alteration (initiated in acid pH)	83 ± 7.0[a]	99 ± 10[a]	9.7×10^{-8}[b] $= 2.7389 \times 10^{-10}$ mol m^{-2} s^{-1}	0.99[a]

$\xi_{extent,max}$ is the maximum value of mineral(s) content or alteration extent at apparent equilibrium and $t_{1/2}$ is the half-content time determined by using a kinetic pseudo-second-order model. v_0 is the initial reaction rate ($v_0 = \xi_{extent,max}/t_{1/2} * 100$).

[a] Values obtained from fitting of a sigmoidal equation ($\xi_{extent} = \xi_{extent,max}/(1 + \exp(-(t - t_{1/2})/b))$).

[b] Effective reaction rate after the so-called incubation period (or induction time) in sigmoidal kinetic behaviors. The alteration rates were normalized with respect to initial specific surface area for olivine fine-grains (2.3 m^2 g^{-1}).

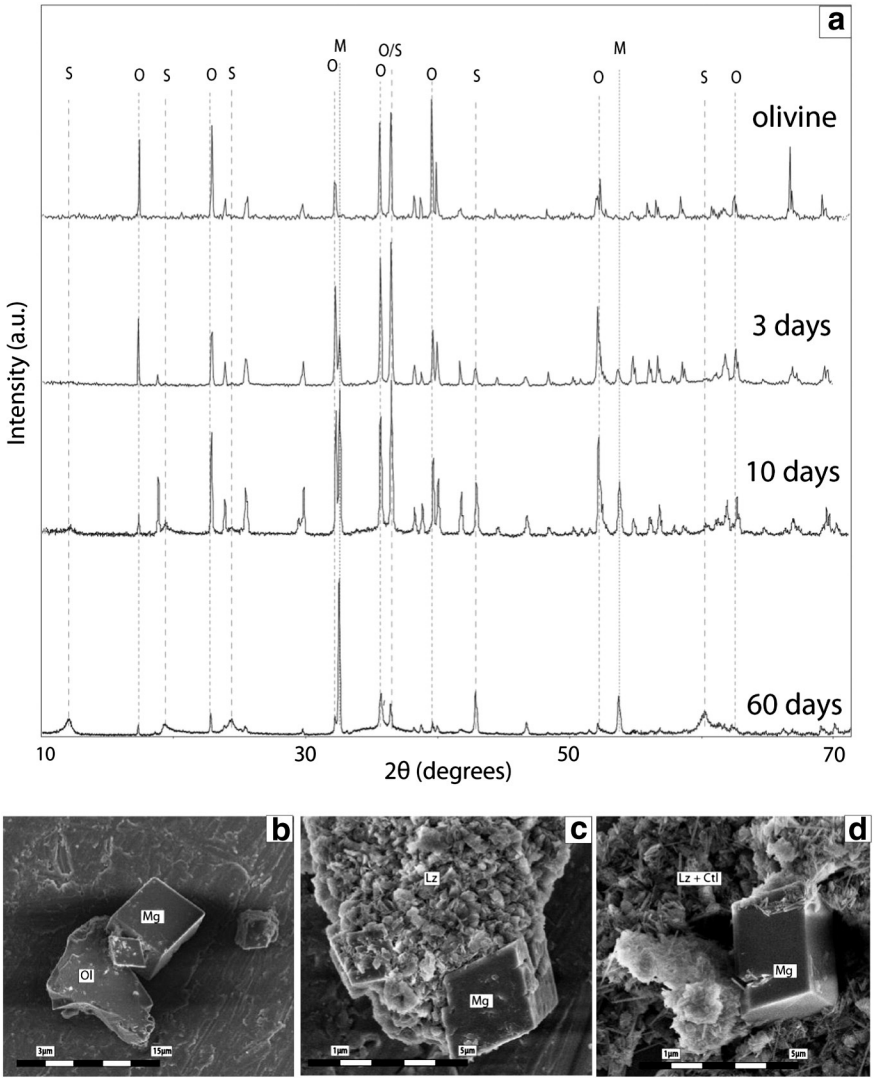

Fig. 1. (a) Experimental X-ray diffraction patterns for starting olivine and for products at different reaction time (3 days: run 1; 10 days: run 2 and 60 days: run 5); S: serpentine, O: olivine, M: magnesite. (b), (c) and (d) FESEM images showing the coexistence of magnesite (Mg) and serpentine (lizardite: Lz and chrysotile: Ctl) during olivine (Ol) alteration after 3 days "run 1" (b), 10 days "run 2" (c) and 60 days "run 5" (d).

competitive serpentinization and carbonation rates reported in the Section 4.2.

Complementary experiments using a serpentinized olivine as starting material (runs 11 to 15), i.e. a mineral material containing chrysotile + brucite + small amount of residual olivine (after Lafay et al., 2012), have revealed a fast carbonation of existing brucite, leading to magnesite formation (see Fig. 4). Conversely, insignificant structural effect was measured/observed for interacting chrysotile by using XRD, IR and FESEM. This was experimentally confirmed by using high-purity chrysotile as starting material in other specific experiments (runs 6 to 10) at the same hydrothermal conditions as qualitatively measured by infrared spectroscopy (Fig. 5). This solid characterization suggests that chrysotile remains close to equilibrium with respect to interacting solution at the investigated conditions.

4. Discussion

4.1. Reaction steps

In a previous recent study, we reported that the serpentinization of San Carlos olivine under high-hydroxyl alkalinity "or high-basic conditions" (pH = 13.5 ex-situ measured at 20 °C) takes place via mineral replacement of olivine by chrysotile and brucite assemblage, i.e. a spatial and temporal coupling of dissolution and precipitation reactions at the interface between olivine and chrysotile–brucite minerals, leading to preservation of external shape of olivine grains (Fig. 6a). For more specific details refer to Lafay et al., 2012. Conversely, in the present study using the same pressure–temperature conditions, but, now using CO_2-rich alkaline solutions (S1 and S2) "or high-carbonate alkalinity", the above mineral replacement reactions has not taken place. In other terms, the original external shape of olivine grains was not preserved as observed by FESEM observations (see for ex. Fig. 6d). These observations suggest that the super-saturation for precipitating minerals (magnesite, lizardite and chrysotile) is also reached into the bulk interacting solution, leading to the precipitation of single magnesite crystals and fine particles of serpentine from solution, i.e. that the mineral dissolution was temporally and spatially decoupled of precipitation reactions. However, the nucleation and epitaxial growth processes at the olivine–fluid interfaces cannot be excluded in our investigated system. As mentioned above, competitive precipitation of magnesite and serpentine were clearly determined on solid products; for more simplicity, i.e. excluding the fate of the iron initially contained in olivine, the

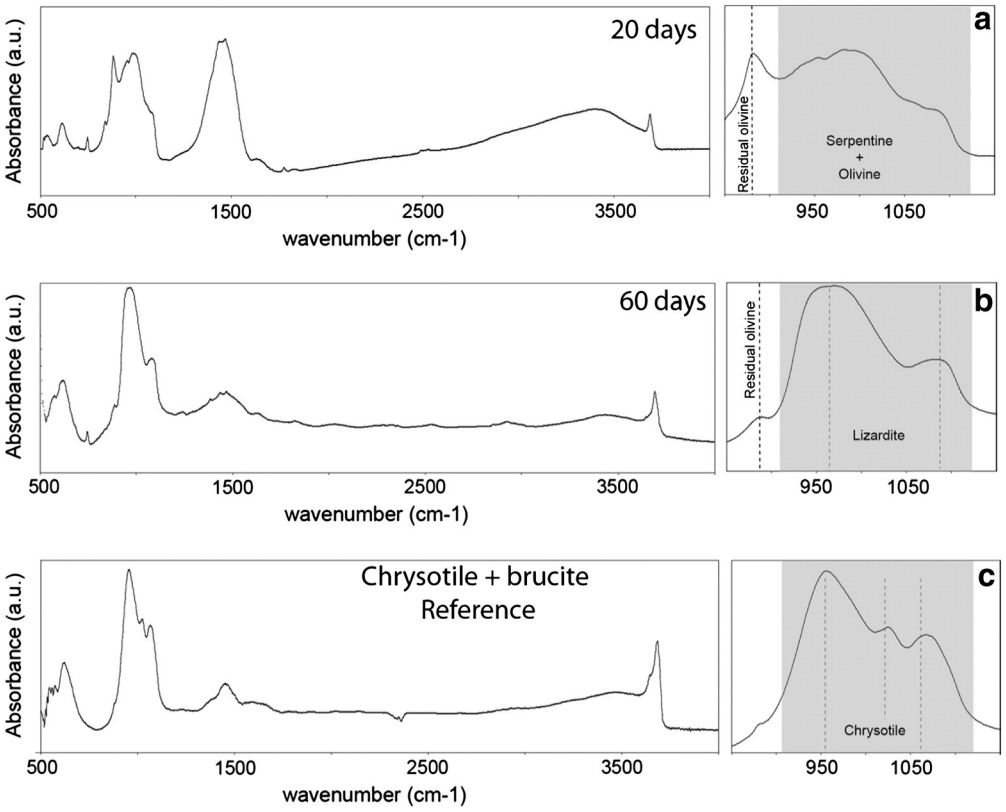

Fig. 2. Infrared measurements (in transmission option) showing a preferential lizardite formation under high-carbonate alkalinity (panel a "run 3" and b "run 5") as attested by their two typical stretching infrared modes at 966 and 1085 cm^{-1} for Si–O group (panel b). These infrared features are clearly different to infrared features of chrysotile polymorph (panel c).

alteration reaction for olivine under high-carbonate alkalinity can be expressed as follows:

$$2Mg_2SiO_4 + 2H_2O + HCO_3^- \rightarrow MgCO_3 + Mg_3Si_2O_5(OH)_4 + OH^-. \quad (2)$$

This reaction mechanism implied a dissolution process, releasing Mg and Si ions into solution until supersaturation of solution with respect to magnesite and/or serpentine. Their kinetic behavior depends directly on the fluid chemistry such as gradual consumption of dissolved carbonate species and in-situ OH^- regeneration in this closed system. This change of fluid chemistry can probably promote the chrysotile formation at the end of the experiment as observed on FESEM images (Fig. 1d). This is possibly due to a decrease of carbonate alkalinity (consumption of HCO_3^-) which is directly proportional to an increase of hydroxyl alkalinity as illustrated in reaction (2). Moreover, recently Lafay et al. (2012) has reported that chrysotile formation is favored under high-hydroxyl alkalinity.

On the other hand, the released iron contained in the olivine has not implied any precipitation of iron oxides or (oxy)hydroxides for runs 1 to

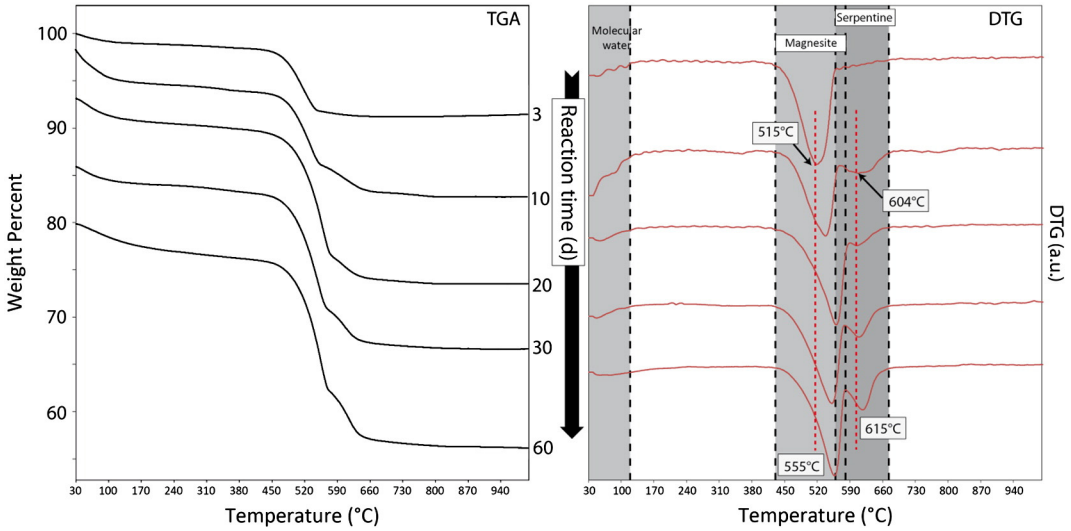

Fig. 3. Thermogravimetric analyses (TGA) on the samples collected at different reaction time and its respective 1st derivative curve (DTG) that enables a temporal quantification of coexisting magnesite and serpentine in the samples (runs 1 to 5, see also Table 1 that summarizes all TGA values). Magnesite and serpentine decomposition seem to be shifted from 515 to 555 °C and from 604 to 615 °C, respectively (DTG graphs); probably due to a progressive crystal size evolution and/or mineral proportion.

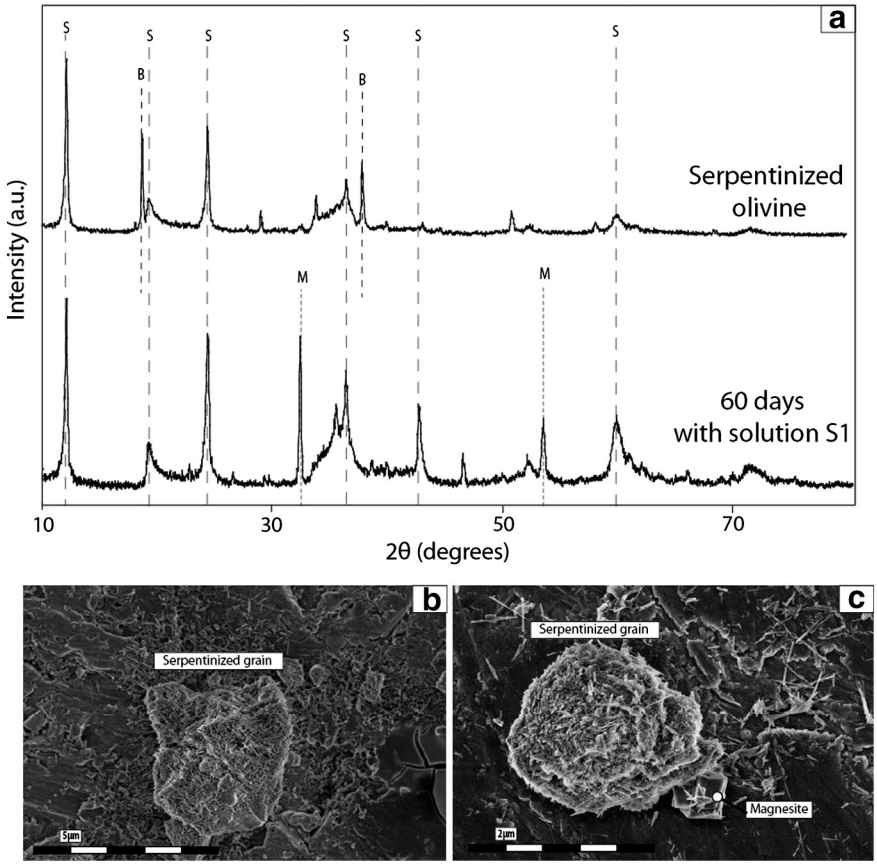

Fig. 4. Reactivity of serpentinized olivine (chrysotile + brucite + small amount of residual olivine as starting material) in high-carbonate alkalinity at 200 °C. XRD patterns for starting material and after 60 days of reaction (run 15) show only brucite-to-magnesite transformation (a) in agreement with FESEM observations. (b) Starting material and (c) after 60 days of reaction (run 15).

5 and 16 to 20; in fact, the released iron was partially oxidized (about 50%) via a simple reduction of water ($2Fe^{2+} + 2H_2O \rightarrow 2Fe^{3+} + H_2 + 2OH^-$). In this way, the released iron was incorporated in serpentine (as Fe(II) and Fe(III)) and in magnesite (as Fe(II) only). This latter is clearly determined by FESEM/EDS chemical analysis on the single magnesite crystals (Fig. 7 concerning run 5).

4.2. Kinetics

The kinetic pseudo-first-order and pseudo-second-order models have been widely used to describe several physicochemical reactions at solid–fluid interfaces such as uptake processes of ions and molecules, photocatalytic oxidation of organic molecules, sorption of vapor water in/on clays, osmotic swelling process of clays, aqueous carbonation of alkaline minerals and crystal growth processes (e.g. Ho and McKay, 1999; Montes-H and Geraud, 2004; Montes-H, 2005; Ho, 2006; Montes-Hernandez et al., 2009a,b, 2010b). In the present study, the kinetic pseudo-second-order model was specifically used to describe the kinetic behavior of olivine alteration under hydrothermal conditions (reaction 2) by using the variation of formed mineral(s) content or the alteration extent ξ_{extent} (%) with time t (day). As mentioned above, temporal variation of magnesite and serpentine concerning the reaction (2) was directly determined by using thermogravimetric measurements (see Fig. 3 and Table 1). These kinetic data were successfully fitted using a kinetic pseudo-second-order model. This simple model predicts a fast mass transfer followed by a slow equilibration of mass transfer in closed systems. The differential form for this kinetic model can be written as follows:

$$\frac{d\xi_{extent}}{dt} = k_{alteration}\left(\xi_{extent,max} - \xi_{extent}\right)^2 \quad (3)$$

where $k_{alteration}$ is the rate constant of olivine alteration [1/% day], $\xi_{extent,max}$ is the maximum value of formed mineral(s) content or alteration extent at apparent equilibrium [%] and ξ_{extent} is the formed mineral(s) content or alteration extent [%] at any time t [day].

The integrated form of Eq. (3) for the boundary conditions $t = 0$ to $t = t$ and $\xi_{extent} = 0$ to $\xi_{extent} = \xi_{extent}$, is represented by a hyperbolic relationship:

$$\xi_{extent} = \frac{\xi_{extent,max} * t}{\left(\frac{1}{k_{alteration} * \xi_{extent,max}}\right) + t}. \quad (4)$$

Note that the rate constant $k_{alteration}$ (1/% day) has no physical interpretation. For this reason a new parameter can be defined "$(1/k_{alteration} * \xi_{extent,max}) = t_{1/2}$", which represents the duration after which half of the maximum of alteration extent was obtained. The Eq. (4) can be then expressed as follows:

$$\xi_{extent} = \frac{\xi_{extent,max} t}{t_{1/2} + t}. \quad (5)$$

In the current study, $t_{1/2}$ is called "half-extent time" and can be used to calculate the initial-rate of olivine alteration, v_0 [1/day] by using the following expression:

$$v_0 = \frac{\xi_{extent,max}}{100 * t_{\frac{1}{2}}}. \quad (6)$$

Graphically, the initial rate of olivine alteration v_0 is defined as the slope of the tangent line when the time t tends towards zero on the r vs. t curve (see for ex. Montes-Hernandez et al., 2009a,b).

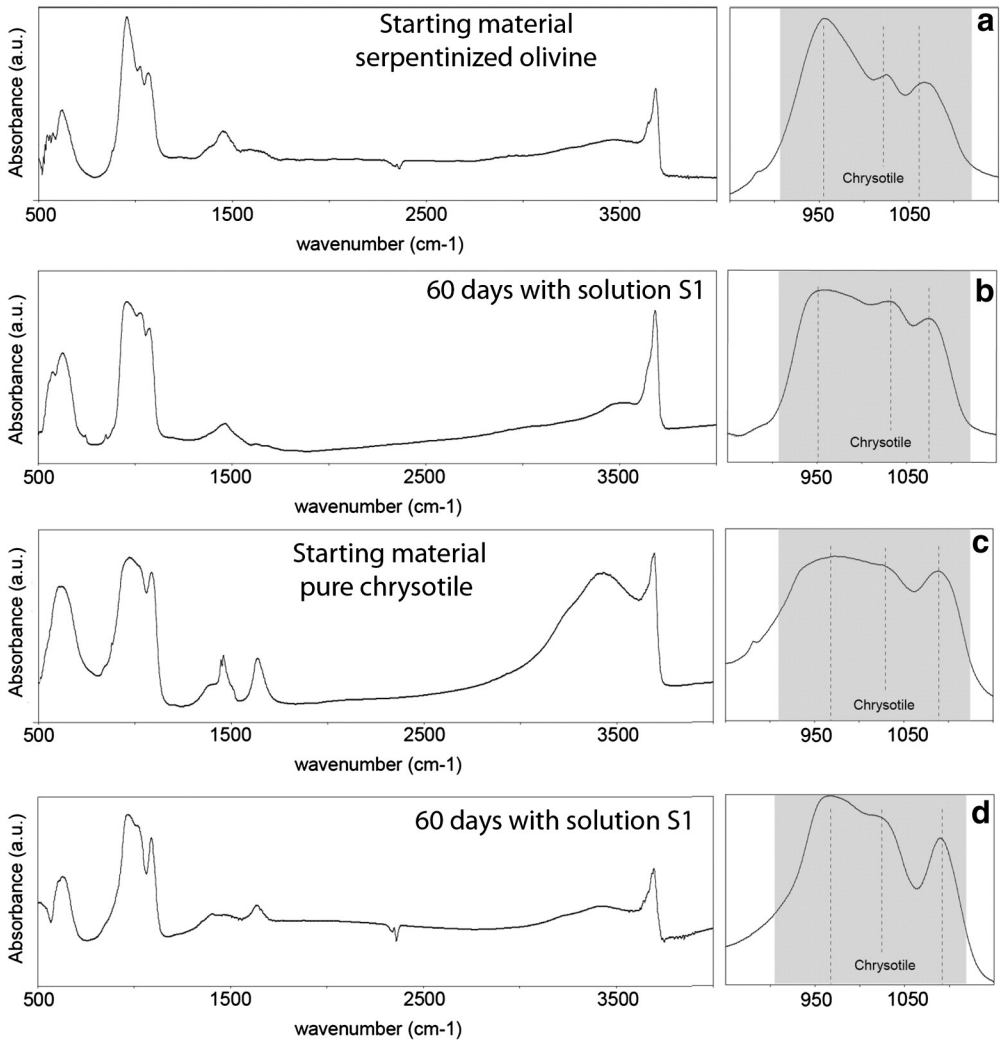

Fig. 5. Infrared measurements confirming slight or insignificant structural changes in reacted chrysotile in high-carbonate alkalinity at 200 °C. Two cases, chrysotile contained in the serpentinized olivine (panels: (a): starting material and (b): after 60 days of reaction "run 15") and high-purity synthetic chrysotile (panels: (c): starting material and (d): after 60 days of reaction "run 10").

A non-linear regression by the least-squares method was performed to determine these two kinetic parameters ($\xi_{extent,max}$ and $t_{1/2}$) from Eq. (5). All values, including correlation factors and initial alteration rates v_0 are summarized in Table 2. We note that the alteration rates were normalized with respect to initial specific surface area for olivine fine-grains (2.3 $m^2\ g^{-1}$) deduced from N_2 adsorption isotherm and applying the conventional Brunauer–Emmett–Teller (BET) equation.

Competitive carbonation (or magnesite formation) and serpentinization (or serpentine formation) concerned in the reaction (2) and displayed in Fig. 8 confirm a retarding process of serpentine formation with respect to magnesite (about three times slower); in fact, the magnesite seems to reach an apparent stabilization after about 20 days of reaction while the serpentine follows a progressive slower evolution. We assumed that the magnesite reaches a fast apparent equilibrium with solution because the available carbonate species are not renewed from gas phase as typically constrained in aqueous carbonation experiments where a given CO_2 pressure is imposed in the system (e.g. Bearat et al., 2006). In this way, the serpentinization process remains active until the end of experiment and the carbonation process seems to be inhibited after about 30 days in the system as shown in Fig. 8. On the other hand, the alteration rate of olivine in the presence of dissolved CO_2 or under high-carbonate alkalinity (1.8636×10^{-9} mol $m^{-2}\ s^{-1}$) is significantly retarded with respect to a CO_2-free system or under high-hydroxyl alkalinity at the same P–T–grain size–solid/fluid ratio conditions (1.6659×10^{-8} mol $m^{-2}\ s^{-1}$) as illustrated in Fig. 9. As invoked above, the chrysotile and brucite were preferentially formed under high-hydroxyl alkalinity and the original external shape of olivine grains was preserved (Lafay et al., 2012). Conversely, under high-carbonate alkalinity, lizardite and magnesite were preferentially formed and the original external shape of olivine grains was not preserved (Fig. 6d).

4.3. Role of pH and fluid chemistry

In a previous recent study, we demonstrated that high-hydroxyl alkalinity (1 M NaOH, pH = 13.5 at 20 °C) promote a fast serpentinization process of San Carlos olivine (Lafay et al., 2012), if it is compared with experimental serpentinization of olivine in high-purity water or in salt solution (seawater analog) already reported by Malvoisin et al. (2012). This latter study has clearly described the influence of temperature and initial grain size on the serpentinization rate. In general, the serpentinization rate increases with a decrease of initial grain size and an increase of temperature from 200 to 350 °C (Malvoisin et al., 2012). However, the serpentinization rate of olivine can also depend on the fluid/solid ratio, fluid hydrodynamics and fluid chemistry (including pH) as suggested by field fluid monitoring and modeling studies (e.g. Charlou et al., 2002; Früh-Green et al., 2003; Allen and Seyfried, 2004; Ludwig et al., 2006; Seyfried et al., 2011). In

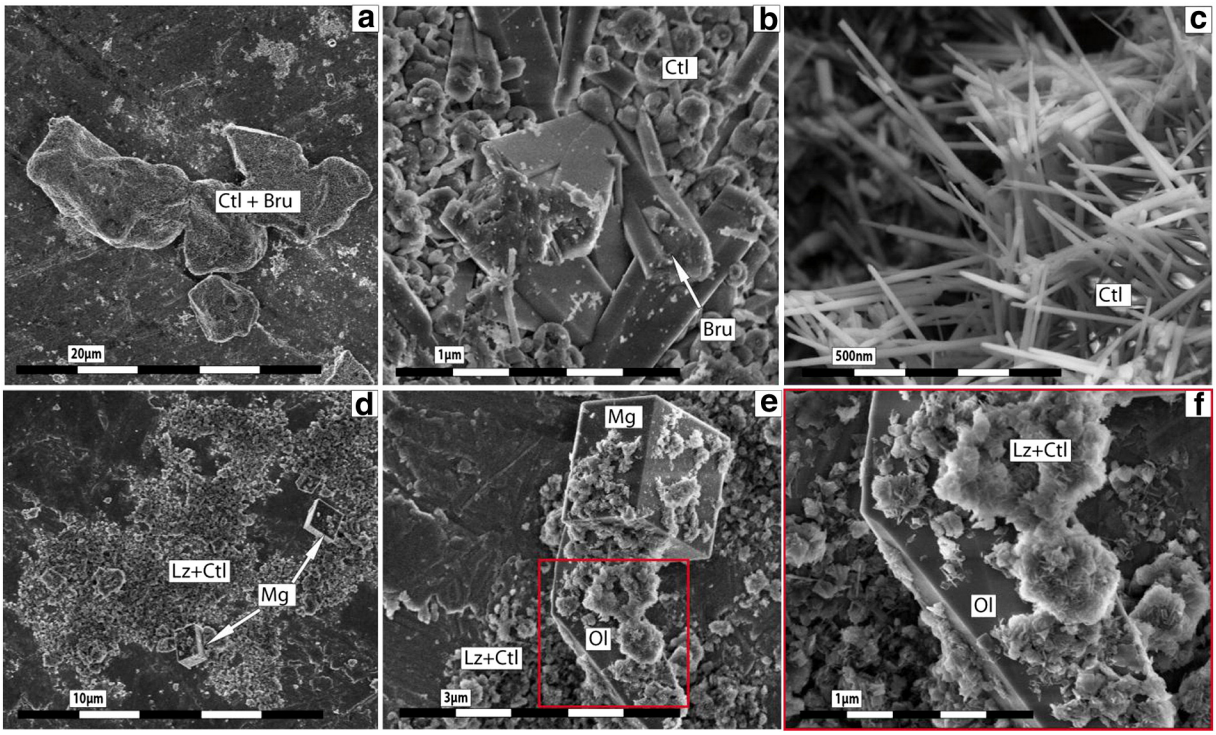

Fig. 6. FESEM images: (a), (b) and (c) show mineral replacement of olivine by chrysotile and brucite under high-hydroxyl alkalinity, implying the preservation of original external shape of olivine grains (image (a), see also Lafay et al., 2012). (d), (e) and (f) show the coexistence of magnesite and serpentine precipitation during olivine alteration under high-carbonate alkalinity without preservation of original external shape of olivine grains (run 5).

this way, the present study has revealed that a simple change in alkalinity from high-hydroxyl alkalinity (1 M NaOH, pH = 13.5 at 20 °C) to high-carbonate alkalinity (1 M $NaHCO_3$, pH = 8.9 at 20 °C) retards significantly the alteration process of olivine (Fig. 9), leading to a preferential formation of lizardite and magnesite. Moreover, the spatial and temporal coupling of dissolution and precipitation reactions (or mineral replacement reactions) was not observed under high-carbonate alkalinity. This means that the fluid chemistry and pH play an important role on the alteration kinetics, reaction mechanisms and nature of solid–gas products during olivine alteration in natural hydrothermal systems. The effect of pH on the dissolution rate of olivine and/or of forsteritic olivine has been assessed using continuous, semi-continuous or discontinuous experimental systems (e.g. Chen and Brantley, 2000; Pokrovsky and Schott, 2000; Rosso and Rimstidt, 2000; Hänchen et al., 2006; Daval et al., 2011). However, the effect of pH on the serpentinization rate for olivine is more difficult to be experimentally assessed because it implies dissolution of primary components followed by precipitation of secondary mineral phases and H_2 production whether redox reactions are significant (e.g. Marcaillou et al., 2011; Lafay et al., 2012; Malvoisin et al., 2012). In an effort, to evaluate the pH effect on the serpentinization rate, the olivine serpentinization was recently investigated under high-hydroxyl alkalinity (pH = 13.5 at 20 °C) (Lafay

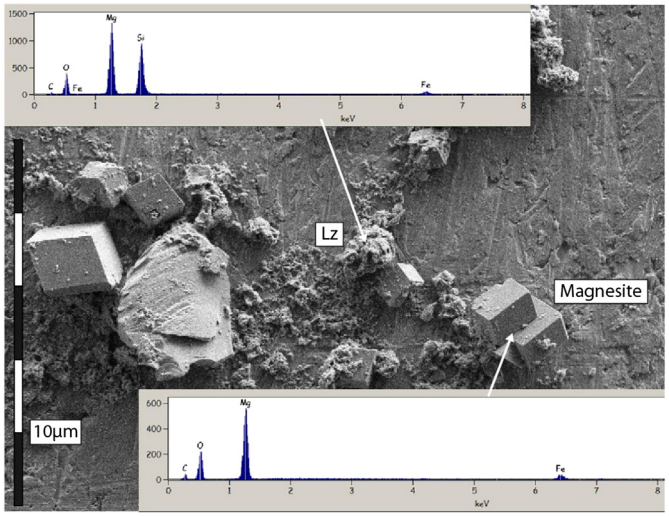

Fig. 7. FESEM/EDS chemical analyses have revealed complex fate of released iron initially contained in San Carlos olivine. Iron content in magnesite suggests partial iron oxidation via water reduction (sample concerning the run 5).

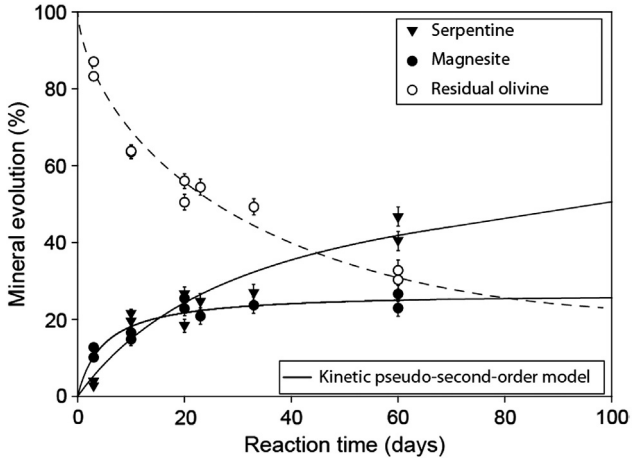

Fig. 8. Competitive kinetic behavior of magnesite and serpentine during olivine alteration under high-carbonate alkalinity (runs 1 to 5 and 16 to 20). Experimental kinetic data for magnesite and serpentine were fitted by using a kinetic pseudo-second-order model and kinetic parameters are reported in Table 2.

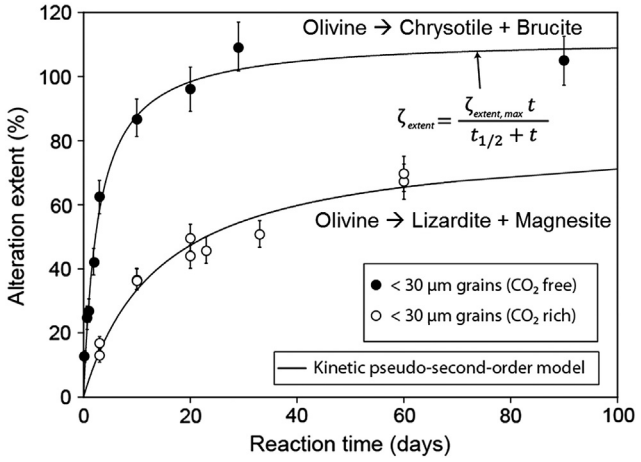

Fig. 9. Alteration kinetic of olivine under high-hydroxyl alkalinity (circles filled) (from Lafay et al., 2012) and under high-carbonate alkalinity (open circles) (from runs 1 to 5 and 16 to 20). Experimental kinetic data were fitted by using a kinetic pseudo-second-order model and kinetic parameters are reported in Table 2.

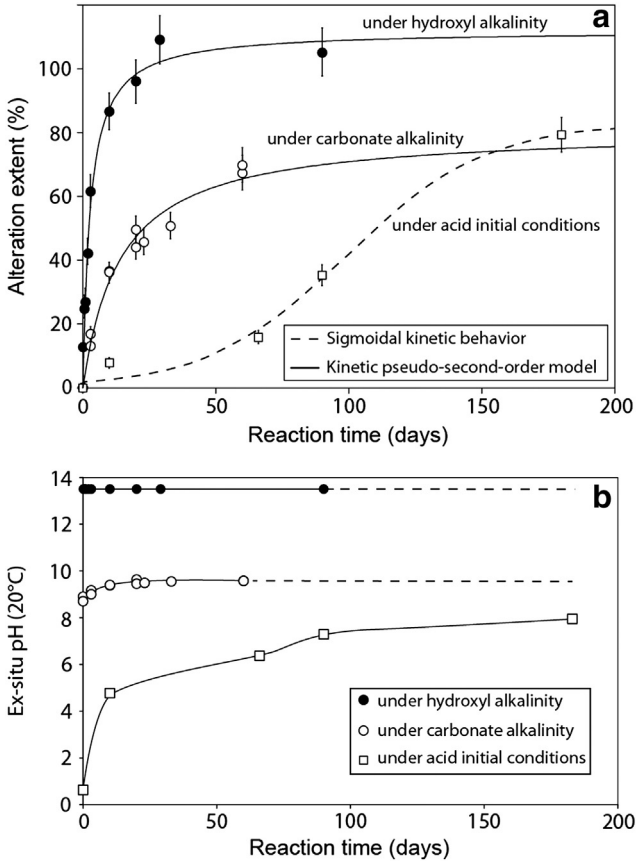

Fig. 10. (a) Alteration kinetic of olivine under high-hydroxyl alkalinity (circles filled) (from Lafay et al., 2012), under high-carbonate alkalinity (open circles) (from runs 1 to 5 and 16 to 20) and initiated in acid pH (open squares) (from runs 21 to 24). (b) pH evolution for each scenario measured ex-situ at room temperature ≈ 20 °C.

et al., 2013). This extreme scenario has provided interesting insights on the kinetics and reaction mechanism. For example, the magnetite (Fe_3O_4) secondary mineral phase, typically observed from olivine serpentinization in high-purity water at T > 200 °C (Marcaillou et al., 2011; Malvoisin et al., 2012) was not observed under high-hydroxyl alkalinity. However, the magnetite formation during serpentinization is frequently related to redox reactions and/or H_2 production (McCollom and Bach, 2009; Marcaillou et al., 2011); herein, we note that the H_2 production is not necessarily associated to magnetite precipitation because it can be produced by simple oxidation of Fe(II) (initially contained in olivine) followed by a simple reduction of water as expressed by the following coupled oxidation–reduction reaction ($2Fe^{2+} + 2H_2O \rightarrow 2Fe^{3+} + H_2 + 2OH^-$). In fact, the oxidized iron (Fe(III)) and reduced iron (Fe(II)) can be selectively incorporated and/or sequestered in major secondary phases (serpentine, brucite, magnesite…) (e.g. Klein et al., 2009; Lafay et al., 2012; this study); this limits the formation of iron oxides and/or oxyhydroxides in specific environments. Under high alkalinity, preliminary Mössbauer spectroscopy measurements (results not shown here) on two selected samples have revealed a partial iron oxidation (≈50%) from Fe(II) to Fe(III) of initial iron contained in olivine. Moreover, FESEM/EDS chemical analyses have revealed that single crystals of magnesite contain significant amount of iron. We note that only Fe(II) can be incorporated into magnesite crystals; this confirms also a partial oxidation. Based on this result, the H_2 production is expected in our system and could be roughly quantified, but, this specific study was mainly oriented on the simultaneous serpentinization and aqueous carbonation of olivine.

On the other hand, some serpentinization experiments (runs 21 to 24 in Table 1) under high-acidic solutions (initial pH = 0.66) have revealed slower serpentinization rates and a more complex kinetic behavior (sigmoidal kinetic behavior: $[\xi_{extent} = \xi_{extent,max}/(1 + \exp(-(t - t_{1/2})/b))]$) than under high-hydroxyl alkalinity (Lafay et al., 2012) and under high-carbonate alkalinity (this study); however, as expected, the pH increases proportionally with serpentinization progress (see Fig. 10), because by definition the dissolution of olivine (ultrabasic rock) in acidic solutions and in discontinuous (or closed) systems, implies a transient consumption of protons (H^+) and the production of hydroxyl ions (OH^-) until the solution supersaturation with respect to serpentine, brucite and other minor mineral phases (e.g. TOT clays and iron oxides/oxyhydroxides). The brucite mineral ($Mg(OH)_2$) is a direct proof of hydroxyl ion production in the system. A simplified reaction mechanism for serpentinization of olivine in acidic solution and in batch system, i.e. excluding the fate of initial Fe(II) contained in olivine, can be expressed as follows:

Dissolution step,

$$2Mg_2SiO_4 + 4H_2O + 4H^+ \rightarrow 4Mg^{2+} + 2H_4SiO_{4(aq)} + 4OH^-. \quad (7a)$$

Precipitation from solution and/or nucleation-growth processes at olivine–fluid interfaces,

$$4Mg^{2+} + 2H_4SiO_{4(aq)} + 4OH^- \rightarrow Mg_3Si_2O_5(OH)_4 + Mg(OH)_2 + H_2O + 4H^+. \quad (7b)$$

The summation of these two reaction steps (7a) and (7b) gives a classic serpentinization global reaction for forsteritic olivine as described in many previous studies:

$$2Mg_2SiO_4 + 3H_2O \rightarrow Mg_3Si_2O_5(OH)_4 + Mg(OH)_2. \quad (7c)$$

This global serpentinization reaction for San Carlos olivine, initiated at low pH (=0.66), is in agreement with thermogravimetric measurements reported in Table 1 (runs 21 to 24) and in Fig. 10. However, we note that minor other mineral phases were also identified from XRD patterns in these experiments such as the hydro-hematite and TOT clay (talc type).

4.4. Is "silica passivating layer" a universal process during olivine alteration?

The formation of passivating layers during solid–fluid interfacial processes are widely documented in materials sciences and chemical engineering areas. For example, in gas–solid carbonation of alkaline sorbents, the CO_2–sorbent reaction typically takes place by the formation of a dense non-porous layer of carbonate (or protective carbonate layer) around the reacting particles. For these cases, the carbonation reaction is generally stopped before a complete carbonation (e.g., Fernandez Bertos et al., 2004; Sun et al., 2008; Huntzinger et al., 2009; Prigiobbe et al., 2009a,b; Stendardo and Foscolo, 2009). Conversely, recent studies have demonstrated that the formation of a so-called passivating layer of carbonate depend strongly on the intrinsic textural properties of reacting particles and on the experimental conditions such as relative humidity, CO_2 pressure, fluid dynamics and temperature (e.g. Beruto and Botter, 2000; Dheilly et al., 2002; Seo et al., 2007; Zeman, 2008; Montes-Hernandez et al., 2010a,b, 2012a,b). In this way, the formation of a protective carbonate layer leads to a physical increase in volume at the grain scale (expansion or swelling process) or a decrease in porosity (pore closure process) when porous materials are partially carbonated (Fernandez Bertos et al., 2004; Chen et al., 2007; Sun et al., 2008). Concerning the olivine aqueous alteration under acid conditions or under high CO_2 pressure (>20 bar), incongruent dissolution process has been measured, leading to a Si-rich layer alteration profile around reacting olivine grains (e.g. Wogelius and Walther, 1991; Pokrovsky and Schott, 2000; Rosso and Rimstidt, 2000; Prigiobbe et al., 2009a, 2009b); its progressive formation generally leads to a passivating effect "limiting reaction process". Similar to gas–solid carbonation process, the formation of a silica layer around the olivine reacting particles could passivate or squarely stopper the interfacial reaction as already invoked by Daval et al., 2011. However, the mechanistic pathway of its formation is still debated in the literature; some authors have proposed a polymerization process via an ion-exchange reaction ($Mg^{2+} \leftrightarrow 2H^+$) and formation of surface ($\equiv Si(OH)_4$) monomers that polymerize to a porous or non-porous silica layer (e.g. Wogelius and Walther, 1991; Chen and Brantley, 2000; Pokrovsky and Schott, 2000; Bearat et al., 2006). Conversely, other recent studies have proposed a temporal and spatial coupling of Si release ($H_4SiO_{4(aq)}$) and silica precipitation process ($SiO_{2(s)}$ layer) (e.g. Daval et al., 2011), initially proposed by Hellmann et al. (2003) for labradorite feldspar altered under acid pH. This implies that the silica phase reaches a rapid supersaturation near of the reacting mineral phase. In this context and based on our recent results (Lafay et al., 2012 and this study), we assume that a silica passivating layer during alteration of olivine is only formed under high acid conditions (pH < 4), including high CO_2 pressure (>20 bar) because under high hydroxyl or carbonate alkalinity conditions (9 < pH ≤ 13.5), the formation of so-called silica passivating layer was not determined/suspected by XRD, FTIR and TGA measurements. This observation is in agreement with a previous study and explanations provided by Pokrovsky and Schott (2000).

5. Coexistence of carbonation and serpentinization processes: from experimentation to natural systems

In the last decades, the serpentinization of olivine have been intensively investigated at the lab scale in order to determine the reaction mechanisms and kinetics, the reaction and cracking propagation from the grain boundaries, its potential for hydrogen production and its implications on the early Earth life, i.e. its role on the abiotic formation of organic molecules (MacLeod et al., 1994; James et al., 2003; Seyfried et al., 2007; McCollom and Bach, 2009; Hövelmann et al., 2011; Marcaillou et al., 2011; Lafay et al., 2012; Malvoisin et al., 2012). Obviously, these studies have direct relevance in Earth systems, but, they are systematically oriented to investigate the olivine alteration in high-purity water, in saline water (seawater analog) or in acidic solutions. In this way, we demonstrated that the olivine alteration under high alkalinity conditions follows different reaction mechanisms and the kinetic behavior is drastically modified as explained above. On the other hand, direct and indirect aqueous carbonation of olivine is intensively being investigated in order to determine the best experimental conditions for ex-situ mineral sequestration of CO_2 using natural olivine. Herein, the Albany Research Centre has reported that the optimum sequestration reaction conditions observed to date are 1 M NaCl + 0.64 M $NaHCO_3$ at T ≈ 180 °C and P_{CO2} ≈ 135 bar (Bearat et al., 2006; Chen et al., 2006; King et al., 2010; Daval et al., 2011). In this context, Bearat et al. (2006) have concluded that mitigating passivating layer effectiveness is critical to enhancing carbonation and lowering sequestration process cost. Inspired on these independent results of olivine serpentinization and aqueous carbonation, specific novel experimental conditions were used in this study (1 M $NaHCO_3$ solution, pH ≈ 9, 200 °C and saturated vapor pressure) in order to investigate a competitive effect between serpentinization and aqueous carbonation of olivine. These simple experimental constraints could contribute to a better understanding of fluid–rock interactions in natural active hydrothermal Earth fields such as Samail Ophiolite in Oman and New Caledonia Ophiolite where a simultaneous serpentinization and aqueous carbonation processes are currently expected (e.g. Kelemen and Matter, 2008; Matter and Kelemen, 2009).

6. Implications for in-situ carbonation of peridotite for CO_2 storage

Unregulated CO_2 emissions into the Earth's atmosphere (about 22×10^9 ton CO_2 $year^{-1}$), caused mainly by fossil fuel combustion, have led to concerns about global warming. To maintain the atmospheric CO_2 level below 500 ppm, CO_2 emissions will have to be stabilized at current levels, although they are forecast to double over the next 50 years (Allwood et al., 2010). Captured from individual industrial sources and long-term geological storage are realistic and available ways of reducing CO_2 emissions because large volumes of this gas can be stored in various deep geological formations (e.g. Knauss et al., 2005; Friedmann, 2007; IPCC, 2007; Bachu, 2008). Recently, Kelemen and Matter (2008) have proposed the in-situ carbonation of peridotite for CO_2 storage, i.e. the injection of purified CO_2 in peridotite massifs. This conceptual methodology requires obviously drilling, hydraulic fracturing, using $NaHCO_3$ as catalyst, pumping fluid and preheating fluid for the first heating step. In this way, the authors have estimated very fast carbonation of peridotite compared with natural peridotite hydration and carbonation in the Samail Ophilite (Oman) and have reported that the in-situ carbonation of peridotite could consume >1 billion tons of CO_2 $year^{-1}$ in Oman alone. In this context, the basic research in the coming years on the simultaneous hydration (and/or serpentinization) and carbonation rates of peridotite "from strategic fields" could have relevant implications for this promising potential alternative for CO_2 storage. In addition, sophisticated experimental setups could be designed to evaluate hydraulic fracturing and reactive percolation in fractured-porous media under high confinement pressure and temperature in order to evaluate the swelling process and associated micro-fracturing related to hydration and/or carbonation processes of peridotite. Technically, this is feasible because various percolation experiments simulating the reactivity of supercritical CO_2 have already been reported (e.g. Le Guen et al., 2007; Andreani et al., 2009).

7. Conclusion

The coexistence of serpentinization and aqueous carbonation of ultrabasic rocks has up to now not been investigated at laboratory scale and various questions still remain unanswered concerning its mechanistic pathways in natural systems, mainly under high alkalinity. In response to this scientific gap, this study provides new insights on competitive serpentinization and aqueous carbonation of olivine under high-carbonate alkalinity. In this way, we quantified a retarding

process of serpentine formation with respect to magnesite (about three times slower) by using a simple kinetic pseudo-second-order model; in fact, the magnesite seems to reach an apparent stabilization after about 20 days of reaction while the serpentine follows a progressive slower evolution. We assumed that the magnesite has reached a fast apparent equilibrium with solution because the available carbonate species are not renewed from fluid phase as typically constrained in aqueous carbonation experiments where a given CO_2 pressure is imposed in the system. In summary, we demonstrated that a simple change of fluid chemistry (including pH) has a significant impact on the reaction mechanism and kinetics for olivine alteration at a given temperature. Some FESEM/EDS chemical analyses and preliminary Mössbauer measurements have revealed that about 50% of initial Fe(II) was oxidized to Fe(III). The not oxidized iron in solution (Fe(II)) from reacting olivine was preferentially incorporated into magnesite crystals. This means a classic hydrogen production via a simple water reduction. The full quantification of redox reactions during simultaneous serpentinization and carbonation of olivine and peridotite under high carbonate alkalinity remains a future challenge.

Acknowledgments

The authors are grateful to the French National Center for Scientific Research (CNRS/INSU), the University Joseph Fourier in Grenoble and ANR French research agency (ANR CORO and ANR SPRING projects) for providing financial support.

References

Allen, D.E., Seyfried Jr., W.E., 2004. Sepentinization and heat generation: constraints from Lost City and Rainbow hydrothermal systems. Geochim. Cosmochim. Acta 68, 1347–1354.
Allwood, J.M., Cullen, J.M., Milford, R.L., 2010. Options for achieving a 50% cut in industrial carbon emissions by 2050. Environmental science & technology 44 (6), 1888–1894.
Andreani, M., Luquot, L., Gouze, P., Godard, M., Hoisé, E., Gibert, B., 2009. Experimental study of carbon sequestration reactions controlled by the percolation of CO_2-rich brine through peridotites. Environ. Sci. Technol. 43, 1226–1231.
Bachu, S., 2000. Sequestration of CO_2 in geological media: criteria and approach for site selection in response to climate change. Energy Convers. Manage. 41, 953–970.
Bachu, S., 2008. CO_2 storage in geological media: role, means, status, barriers to deployment. Prog. Energy Combust. Sci. 34, 254–273.
Bearat, H., Mckelvy, M.J., Chizmeshya, A.V.G., Gormley, D., Nunez, R., Carpenter, R.W., Squires, K., Wolf, G.H., 2006. Carbon sequestration via aqueous olivine mineral carbonation: role of passivating layer formation. Environ. Sci. Technol. 40, 4802–4808.
Beruto, D.T., Botter, R., 2000. Liquid-like H_2O adsorption layers to catalyse the $Ca(OH)_2$/CO_2 solid–gas reaction and to form a non-protective solid product layer at 20 °C. J. Eur. Ceram. Soc. 20, 497–503.
Bonfils, B., Julcour-Lebigue, C., Guyot, F., Bodénan, F., Chiquet, P., Bougeois, F., 2012. Comprehensive analysis of direct aqueous mineral carbonation using dissolution enhancing organic additives. Int. J. Greenhouse Gas Control 9, 334–346.
Charlou, J.L., Donval, J.P., Fouquet, Y., Jean-Baptiste, P., Holm, N., 2002. Geochemistry of high H_2 and CH_4 vent fluids issuing from ultramafic rocks at the Rainbow hydrothermal field (36° 14′N, MAR). Chem. Geol. 191, 345–359.
Chen, Y., Brantley, S.L., 2000. Dissolution of forsteritic olivine at 65 °C and 2 < pH < 5. Chem. Geol. 165, 267–281.
Chen, Z.-Y., O'Connor, W.K., Gerdemann, S.J., 2006. Chemistry of aqueous mineral carbonation for carbon sequestration and explanation of experimental results. Environ. Prog. 25, 161–166.
Chen, M., Wang, N., Yu, J., Yamaguchi, A., 2007. Effects of porosity on carbonation and hydration resistance of CaO materials. J. Eur. Ceram. Soc. 27, 1953–1959.
Daval, D., Sissmann, O., Menguy, N., Saldi, G.D., Guyot, F., Martinez, I., Corvisier, J., Garcia, B., Machouk, I., Knauss, K.G., Hellmann, R., 2011. Influence of amorphous silica layer formation on the dissolution rate of olivine at 90 °C and elevated pCO_2. Chem. Geol. 284, 193–209.
Dheilly, R.M., Tudo, J., Sebai, Y., Queneudec, M., 2002. Influence of storage conditions on the carbonation of powdered $Ca(OH)_2$. Constr. Build. Mater. 16, 155–161.
Fernandez Bertos, M., Simons, S.J.R., Hills, C.D., Carey, P.J., 2004. A review of accelerated carbonation technology in the treatment of cement-based materials and sequestration. J. Hazard. Mater. B112, 193–205.
Friedmann, S.J., 2007. Geological carbon dioxide sequestration. Elements 3, 179–184.
Fritz, B., Clément, A., Montes-Hernandez, G., Noguera, C., 2013. Calcite formation by hydrothermal carbonation of portlandite: complementary insights from experiment and simulation. CrystEngComm 15, 3392–3401.
Früh-Green, G.L., Kelley, D.S., Bernasconi, S.M., Karson, J.A., Ludwig, K.A., Butterfield, D.A., Boschi, C., Proskurowski, G., 2003. 30,000 years of hydrothermal activity at the Lost City vent field. Science 301, 495–498.
Garcia, B., Beaumont, V., Perfetti, E., Rouchon, V., Blanchet, D., Oger, P., Dromart, G., Huc, A.-Y., Haeseler, F., 2010. Experiments and geochemical modeling of CO_2 sequestration by olivine: potential, quantification. Appl. Geochem. 25, 1383–1396.
Gerdemann, S.J., O'Connor, W.K., Dahlin, D.C., Penner, L.R., Rush, H., 2007. Ex situ aqueous mineral carbonation. Environ. Sci. Technol. 41, 2587–2593.
Giammar, D.E., Bruant, R.G., Peters, A., 2005. Forsterite dissolution and magnesite precipitation at conditions relevant for deep saline aquifer storage and sequestration of carbon dioxide. Chem. Geol. 217, 257–276.
Hänchen, M., Prigiobbe, V., Storti, G., Seward, T.M., Mazzotti, M., 2006. Dissolution kinetics of forsteritic olivine at 90–150 °C including effects of the presence of CO_2. Geochim. Cosmochim. Acta 70, 4403–4416.
Hellmann, R., Penisson, J.-M., Hervig, R.L., Thomassin, J.-H., Abrioux, M.-H., 2003. An EFTEM/HRTEM high-resolution study of the near surface of labradorite feldspar altered at acid pH: evidence for interfacial dissolution–reprecipitation. Phys. Chem. Miner. 30, 192–197.
Ho, Y.-S., 2006. Review of second-order models for adsorption systems. J. Hazard. Mater. B136, 681–689.
Ho, Y.-S., McKay, G., 1999. Pseudo-second order model for sorption processes. Proc. Biochem. 34, 451–465.
Hövelmann, J., Austrheim, H., Beinlich, A., Munz, I.A., 2011. Experimental study of the carbonation of partially serpentinized and weathered peridotites. Geochim. Cosmochim. Acta 75, 6760–6779.
Huntzinger, D.N., Gierke, J.S., Kawatra, S.K., Eisele, T.C., Sutter, L.L., 2009. Carbon dioxide sequestration in cement kiln dust through mineral carbonation. Environ. Sci. Technol. 43, 1986–1992.
IPCC (Intergovernmental Panel on Climate Change), 2007. Climate Change 2007: Climate Change Impacts, Adaptations and Vulnerability.
James, R.H., Allen, D.E., Seyfried Jr., W.E., 2003. An experimental study of alteration of oceanic crust and terrigenous sediments at moderate temperatures (51 to 350 °C): insights as to chemical processes in near-shore ridge-flank hydrothermal systems. Geochim. Cosmochim. Acta 67, 681–691.
Kaszuba, J.P., Janecky, D.R., Snow, M.G., 2003. Carbon dioxide reaction processes in a model brine aquifer at 200 °C and 200 bars: implications for geologic sequestration of carbon. Appl. Geochem. 18, 1065–1080.
Kaszuba, J.P., Janecky, D.R., Snow, M.G., 2005. Experimental evaluation of mixed fluid reactions between supercritical carbon dioxide and NaCl brine: relevance to the integrity of a geologic carbon repository. Chem. Geol. 217, 277–293.
Kelemen, P.B., Matter, J.M., 2008. In situ carbonation of peridotite for CO_2 storage. Proc. Natl. Acad. Sci. U. S. A. 105, 17295–17300.
Kelemen, P.B., Matter, J.M., Streit, E.E., Rudge, J.F., Curry, W.B., Blusztajn, J., 2011. Rates and mechanisms of mineral carbonation in peridotite: natural processes and recipes for enhanced, in situ CO_2 capture and storage. Annu. Rev. Earth Planet. Sci. 39, 545–576.
Kelley, D.S., Karson, J.A., Blackman, D.K., Früh-Green, G.L., et al., 2001. An off-axis hydrothermal vent field near the Mid-Atlantic Ridge at 30° N. Nature 412, 145–149.
Kelley, D.S., Karson, J.A., Früh-Green, G.L., Yoerger, D.R., et al., 2005. A serpentinite-hosted ecosystem: the Lost City hydrothermal field. Science 307, 1428–1434.
King, H.E., Plümper, O., Putnis, A., 2010. Effect of secondary phase formation on the carbonation of olivine. Environ. Sci. Technol. 44, 6503–6509.
Klein, F., Garrido, C.J., 2011. Thermodynamic constraints on mineral carbonation of serpentinized peridotite. Lithos 126, 126–160.
Klein, F., Bach, W., Jöns, N., McCollomb, T., Moskowitz, B., Berquó, T., 2009. Iron partitioning and hydrogen generation during serpentinization of abyssal peridotites from 15°N on the Mid-Atlantic Ridge. Geochim. Cosmochim. Acta 73, 6868–6893.
Knauss, K.G., Johnson, J.W., Steefel, C.I., 2005. Evaluation of the impact of CO_2, co-contaminant gas, aqueous fluid and reservoir rock interactions on the geological sequestration of CO_2. Chem. Geol. 217, 339–350.
Lackner, K.S., Wendt, C.H., Butt, D.P., Joyce, E.I., Sharp, D.H., 1995. Carbon dioxide disposal in carbonate minerals. Energy 20, 1153–1170.
Lafay, R., Montes-Hernandez, G., Janots, E., Chiriac, R., Findling, N., Toche, F., 2012. Mineral replacement rate of olivine by chrysotile and brucite under high alkaline conditions. J. Cryst. Growth 347, 62–72.
Lafay, R., Montes-Hernandez, G., Janots, E., Chiriac, R., Findling, N., Toche, F., 2013. Nucleation and growth of chrysotile nanotubes in H_2SiO_3–$MgCl_2$–NaOH medium from 90 to 300 °C. Chem. Eur. J. 19, 5417–5424.
Le Guen, Y., Renard, F., Hellmann, R., Collombet, M., Tisserand, D., Brosse, E., Gratier, J.-P., 2007. Enhanced deformation of limestone and sandstone in the presence of a high pCO_2 fluids. J. Geophys. Res. 112, B05421. http://dx.doi.org/10.1029/2006JB004637.
Ludwig, K.A., Kelley, D.S., Butterfield, D.A., Nelson, B.K., Früh-Green, G., 2006. Formation and evolution of carbonate chimneys at the Lost City hydrothermal field. Geochim. Cosmochim. Acta 70, 3625–3645.
MacLeod, G., McKeown, C., Hall, A.J., Russell, M.J., 1994. Hydrothermal and oceanic pH conditions of possible relevance to the origin of life. Orig. Life Evol. Biosph. 23, 19–41.
Malvoisin, B., Brunet, F., Carlut, J., Rouméjon, S., Cannat, M., 2012. Serpentinization of oceanic peridotites: 2. Kinetics and processes of San Carlos olivine hydrothermal alteration. J. Geophys. Res. 117, B04102. http://dx.doi.org/10.1029/2011JB008842.
Marcaillou, C., Muñoz, M., Vidal, O., Parra, T., Harfouche, M., 2011. Mineralogical evidence for H_2 degassing during serpentinization at 300 °C/300 bar. Earth Planet. Sci. Lett. 303, 281–290.
Matter, J.M., Kelemen, P.B., 2009. Permanent CO_2 storage and mineral carbonation in geologic reservoirs. Nat. Geosci. 2, 837–841.
McCollom, T.M., Bach, T.M., 2009. Thermodynamic constraints on the hydrogen generation during serpentanization of ultramafic rocks. Geochim. Cosmochim. Acta 73, 856–875.
Montes-H, G., 2005. Swelling-shrinkage measurements of bentonite by using coupled environmental scanning electron microscopy and digital images analysis. J. Colloid Interface Sci. 284, 271–277.

Montes-H, G., Geraud, Y., 2004. Sorption kinetic of water vapour of MX80 bentonite submitted to different physical–chemical and mechanical conditions. Colloids Surf., A 235, 17–23.
Montes-Hernandez, G., Fernandez-Martinez, A., Renard, F., 2009a. Novel method to estimate the linear growth rate of submicrometric calcite produced in a triphasic gas–liquid–solid system. Cryst. Growth Des. 9, 4567–4573.
Montes-Hernandez, G., Perez-Lopez, R., Renard, F., Nieto, J.-M., Charlet, L., 2009b. Mineral sequestration of CO_2 by aqueous carbonation of coal combustion fly-ash. J. Hazard. Mater. 161, 1347–1354.
Montes-Hernandez, G., Pommerol, A., Renard, F., Beck, P., Quirico, E., Brissaud, O., 2010a. In-situ kinetic measurements of gas–solid carbonation of $Ca(OH)_2$ by using an infrared microscope coupled to a reaction cell. Chem. Eng. J. 161, 250–256.
Montes-Hernandez, G., Daval, D., Chiriac, R., Renard, F., 2010b. Growth of nanosized calcite through gas–solid carbonation of nanosized portlandite particles under anisobaric conditions. Cryst. Growth Des. 10, 4823–4830.
Montes-Hernandez, G., Renard, F., Chiriac, R., Findling, N., Toche, F., 2012a. Rapid precipitation of magnesite micro-crystals from $Mg(OH)_2$–H_2O–CO_2 slurry enhanced by NaOH and a heat-ageing step (from 20 to 90 °C). Cryst. Growth Des. 12, 5233–5240.
Montes-Hernandez, G., Chiriac, R., Toche, F., Renard, F., 2012b. Gas–solid carbonation of $Ca(OH)_2$ and CaO particles under non-isothermal and isothermal conditions by using a thermogravimetric analyzer: implications for CO_2 capture. Int. J. Greenhouse Gas Control 11, 172–180.
Oelkers, E.H., Gislason, S.R., Matter, J., 2008. Mineral carbonation of CO_2. Elements 4, 333–337.
Parkhurst, D.L., Appelo, C.A.J., 1999. Users guide to PHREEQC (version 2) — a computer program for speciation, batch reaction, one dimensional transport and inverse geochemical calculations. U.S. Geological Survey Water-Resources Investigation Report 99-4259 (312 pp.).
Pokrovsky, O.S., Schott, J., 2000. Kinetics and mechanism of forsterite dissolution at 25 °C and pH from 1 to 12. Geochim. Cosmochim. Acta 64, 3313–3325.
Prigiobbe, V., Polettini, A., Baciocchi, R., 2009a. Gas–solid carbonation kinetics of air pollution control residues for CO_2 storage. Chem. Eng. J. 148, 270–278.
Prigiobbe, V., Costa, G., Baciocchi, R., Hänchen, M., Mazzoti, M., 2009b. The effect of CO_2 and salinity on olivine dissolution kinetics at 120 °C. Chem. Eng. Sci. 64, 3510–3515.
Rosso, J.J., Rimstidt, D.J., 2000. A high resolution study of forsterite dissolution rates. Geochim. Cosmochim. Acta 64, 797–811.
Rudge, J.F., Kelemen, P.B., Spiegelman, M., 2010. A simple model of reaction-induced cracking applied to serpentinization and carbonation of peridotite. Earth Planet. Sci. Lett. 291, 215–227.
Schrenk, M.O., Brazelton, W.J., Lang, S.Q., 2013. Serpentinization, carbon, and deep life. Rev. Mineral. Geochem. 75, 575–606.
Schwarzenbach, E.M., Früh-Green, G.L., Bernosconi, S.M., Alt, J.G., Plas, A., 2013. Serpentinization and carbon sequestration: a study of two ancient peridotite-hosted hydrothermal systems. Chem. Geol. 351, 115–133.
Seifritz, W., 1990. CO_2 disposal by means of silicates. Nature 345, 486.
Seo, Y., Jo, S.-H., Ryu, C.K., Yi, C.-K., 2007. Effects of water vapour pretreatment time and reaction temperature on CO_2 capture characteristics of a sodium-based solid sorbent in a bubbling fluidized-bed reactor. Chemosphere 69, 712–718.
Seyfried Jr., W.E., Foustoukos, D.I., Fu, Q., 2007. Redox evolution and mas transfer during serpentinization: an experimental and theoretical study at 200 °C, 500 bar with implications for ultramafic-hosted hydrothermal systems at Mid-Ocean Ridges. Geochim. Cosmochim. Acta 71, 3872–3886.
Seyfried Jr., W.E., Pester, N.J., Ding, K., Rough, M., 2011. Vent fluid chemistry of the Rainbow hydrothermal system (36°N, MAR): phase equilibria and in situ pH controls on subseafloor alteration processes. Geochim. Cosmochim. Acta 75, 1574–1593.
Stendardo, S., Foscolo, P.U., 2009. Carbon dioxide capture with dolomite: a model for gas–solid reaction within the grains of a particulate sorbent. Chem. Eng. Sci. 64, 2343–2352.
Sun, P., Grace, J.R., Lim, C.J., Anthony, E.J., 2008. A discrete-pore-size-distribution-based gas–solid model and its application to the CaO + CO_2 reaction. Chem. Eng. Sci. 63, 57–70.
Wogelius, R.A., Walther, J.V., 1991. Olivine dissolution at 25 °C: effects of pH, CO_2, and organic acids. Geochim. Cosmochim. Acta 55, 943–954.
Wunder, B., Schreyer, W., 1997. Antigorite: high-pressure stability in the system MgO–SiO_2–H_2O (MSH). Lithos 41, 213–227.
Xu, W.Y., Apps, J.A., Pruess, K., 2004. Numerical simulation of CO_2 disposal by mineral trapping in deep aquiefers. Appl. Geochem. 19, 917–936.
Zeman, F., 2008. Effect of steam hydration on performance of lime sorbent for CO_2 capture. Int. J. Greenhouse Gas Control 2, 203–209.